Experimental and numerical analysis of the wave propagation through a narrow channel in a wave flume.

G. Dupont,[1,2] O. Kimmoun,[2] and B. Molin[2]

[1] *Institut Fresnel, CNRS, France*
[2] *Centrale Marseille - IRPHE, CNRS, France**

27^{th} *International Workshop on Water Waves and Floating Bodies, Copenhagen, Denmark, April 2012.*

I. INTRODUCTION.

In this paper, we study the effects of a narrow channel in a wave flume on the propagation of weakly nonlinear water waves, both numerically and experimentally. The first motivation for such a work was found in optical community where people [1] study enhanced (or extraordinary) transmission of light by subwavelength apertures. In our case, we just consider one narrow channel and we aim to exhibit resonant effects and transmission features of such a channel.

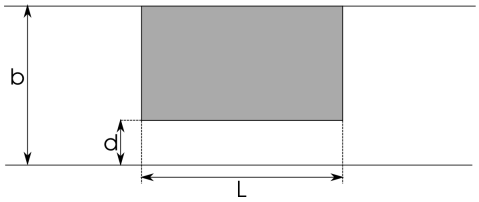

FIG. 1. Top view of the narrowing of the wave flume. In our case, $b = 0.65\,\mathrm{m}$, $L = 0.65\,\mathrm{m}$ and $d \in [10; 1]\,\mathrm{cm}$

For numerical investigations, the framework is weakly nonlinear potential theory up to the second order. Experimentally, waves are generated by a wavemaker in the flume, and some wave gauges are used to measure free-surface elevation, together a video technique.

II. NUMERICAL TOOLS.

The velocity potential is developed to second-order:

$$\Phi(x, y, z, t) = \varepsilon\Phi^{(1)}(x, y, z, t) + \varepsilon^2\Phi^{(2)}(x, y, z, t) \tag{1}$$

where ε is a small parameter identified with the wave steepness.

For harmonic waves with frequency ω and wave number k, the potential writes:

$$\Phi(x, y, z, t) = \mathbb{R}\left\{\varepsilon\phi^{(1)}(x, y, z)\mathrm{e}^{-\mathrm{i}\,\omega t} + \varepsilon^2\phi^{(2)}(x, y, z)\mathrm{e}^{-2\mathrm{i}\,\omega t}\right\} + \varepsilon^2\phi_0^{(2)}(x, y, z) \tag{2}$$

The first order potential is given by:

$$\phi^{(1)}(x, y, z) = -\mathrm{i}\,\frac{A\,g}{\omega}\,\frac{\cosh k(z + h)}{\cosh kh}\,\varphi(x, y) \tag{3}$$

The first-order problem is solved via eigen-function expansions of the velocity potential in the 3 sub-domains, on the weather side of the channel (sub-domain 1, $\infty < x \leq -L/2$), the channel (sub-domain 2, $-L/2 \leq x \leq L/2$), and the lee side (sub-domain 3, $L/2 \leq x < \infty$). The expansions and their x-derivatives are matched on the common boundaries.

*guillaume.dupont@fresnel.fr, olivier.kimmoun@ec-marseille.fr, bernard.molin@ec-marseille.fr

When the wave flume is narrow enough that only one propagative mode exists ($k\,b < \pi$), neglecting the evanescent modes, an approximate analytical solution is obtained as:

$$\begin{array}{rcl} \varphi_1(x) &=& \mathrm{e}^{\mathrm{i}\,k\,x} + A\,\mathrm{e}^{-\mathrm{i}\,k\,(x+L/2)} \\ \varphi_2(x) &=& \mathrm{e}^{\mathrm{i}\,k\,x} + B\,\mathrm{e}^{\mathrm{i}\,k\,(x+L/2)} + C\,\mathrm{e}^{-\mathrm{i}\,k\,(x-L/2)} \\ \varphi_3(x) &=& \mathrm{e}^{\mathrm{i}\,k\,x} + D\,\mathrm{e}^{\mathrm{i}\,k\,(x-L/2)} \end{array} \qquad \left\{ \begin{array}{rcl} B + C &=& \dfrac{\mathrm{i}\,(b-d)\,\sin(kL/2)\,\mathrm{e}^{-\mathrm{i}\,k\,L/2}}{\mathrm{i}\,d\,\sin(kL/2) - b\,\cos(kL/2)} \\ B - C &=& \dfrac{(b-d)\,\cos(kL/2)\,\mathrm{e}^{-\mathrm{i}\,k\,L/2}}{d\,\cos(kL/2) - \mathrm{i}\,b\,\sin(kL/2)} \\ A &=& B + C\,\mathrm{e}^{2\,\mathrm{i}\,k\,L/2} \\ D &=& B\,\mathrm{e}^{2\,\mathrm{i}\,k\,L/2} + C \end{array} \right. \tag{4}$$

The second order potential at the double frequency $2\,\omega$ verifies the free-surface condition:

$$g\phi_z^{(2)} - 4\omega^2\phi^{(2)} = \mathrm{i}\,\omega\left[{\phi_x^{(1)}}^2 + {\phi_y^{(1)}}^2 + \frac{1}{2}k^2 T {\phi^{(1)}}^2\right] \quad ; \quad T = 3\tanh^2(kh) - 1 \tag{5}$$

Here, the second order potential is expressed as a sum of a particular solution verifying the non-homogeneous free-surface condition and a general solution verifying the homogeneous free-surface condition. Numerical resolution is in the same way than for the first order.

Some illustrative numerical results are given in figure 2 below. The length of the channel and the width of the flume are both equal to 0.65 m, while the width of the channel takes 3 different values of 3.2 cm, 2.1 cm and 1 cm. The waterdepth is 25 cm.

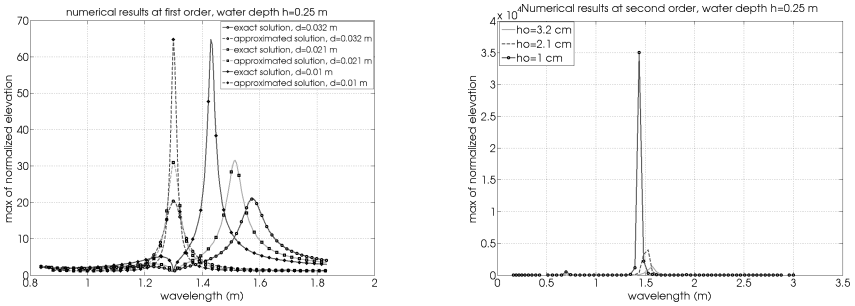

(a)Maximum first order elevation in the narrow channel. Exact and approximate solution.

(b)Maximum second order elevation in the narrow channel.

FIG. 2. Numerical results for maximum free-surface elevation in the narrow channel normalised by the incident wave elevation for the fondamental and the first harmonic.

Figure 2 (a) shows the maximum value of the first-order free surface elevation along the channel, referred to the incident wave amplitude, as a function of the wavelength. According to the analytical solution (4) above, a resonant peak appears at a wavelength equal to twice the flume width (1.3 m) and the peak value is the flume width over channel width ratio b/d. The exact calculations show noticeable shifts. Experimentally much lower free surface elevations are measured at resonance, the main reason being that our potential flow model does not account for dissipative effects. Besides wave breaking, two other effects lead to dissipation: separation at the sharp corners where the corresponding drag force is proportional to the square of the velocity, and friction along the vertical walls where the force is linear in velocity. To select the better dissipation to introduce in our model, the maximum elevation in the narrow channel normalized by the incident wave elevation for the first harmonic is plotted as a function of the steepness in fig.3.

Results suggest that, for large gap and waterdepth, the dissipation is quadratic. For the smallest gap, the dissipation by friction on the wall seems to be larger than the dissipation induced by flow separation at the corners. For smallest depth and gap, wave breaking occurred even for weak steepnesses. In these cases, the wave breaking dissipation is larger than other dissipations.

Consequently, to introduce dissipation in the model, we have added a pressure jump, quadratic with the velocity (via porous screens), at the inlet and outlet of the narrow channel. This trick was used in the first order model only.

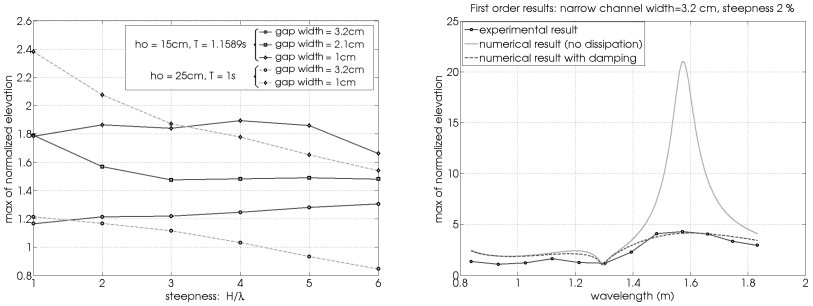

(a)Maximum first order elevation in the narrow channel. Experimental results.

(b)Comparison of experimental data and numerical results with and without damping.

FIG. 3. (a) Maximum elevation in the narrow channel normalised by the incident wave elevation as a function of the steepness. (c) Validation of damping intoduction in numerical model

III. EXPERIMENTAL RESULTS.

A. Set up the problem.

In order to measure the wave elevation, different techniques have been used. First, a set of five resistive wave gauges has been used to separate the amplitude of the incident and the reflected waves. A capacitive wave gauge has been placed after the narrow channel to access to the transmitted waves. To caracterise the free-surface elevation in the channel, fluoresceine has been added to water, and the liquid has been lit by a laser. We have recorded the time evolution of the free-surface with a CCD camera placed on the side of the flume (fig.4).

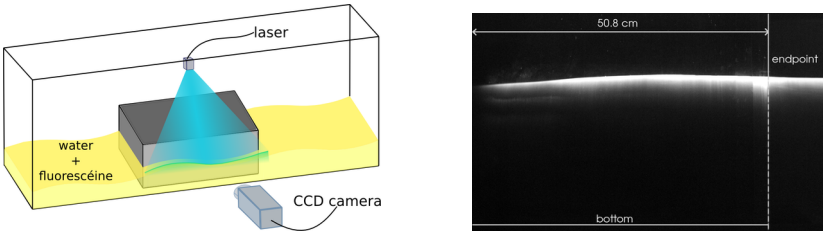

(a)Schematic representation of the experimental setup.

(b)CCD image. Side view of the free-surface elevation at fixed time.

FIG. 4. Experimental setup.

In this work, we have studied six values of the narrow channel width $d = 10,\ 7.8,\ 5.5,\ 3.2,\ 2.1,\ 1\,\text{cm}$ for two water depths $h_0 = 15,\ 25\,\text{cm}$. The wave periods are in the range $[0.75; 1.3]\,\text{s}$.

B. Results.

In figure 5, we present behavior of the free-surface elevation in the narrow channel for $d = 3.2,\ 2.1,\ 1\,\text{cm}$.

The first step consists in a post-treatment of CCD images to access the free-surface elevation η_{fs}. So we can represent the maximum of the normalized free-surface elevation $max(\eta_{fs}^{(1)}/A)$ for the first order, as a function of the wavelength, where A is the incident wave amplitude.

We note a good agreement between numerical and experimental results. The resonant effect occurs as predicted by the theory 2. Behavior is quite similar for the other values of the narrow channel width.

In figure 6, we present the transmission coefficient associated with the narrow channel for $d = 3.2,\ 2.1,\ 1\,\text{cm}$. Here, we used the free-surface elevation measured with the capacitive sensors. The transmission coefficient is plotted as a function of the wavelength and time.

We first observe that the maximum of transmission corresponds to the resonance. Also, we can easily see that the transmission occurs on a larger interval of wavelengths for the smaller water depth and larger channel width.

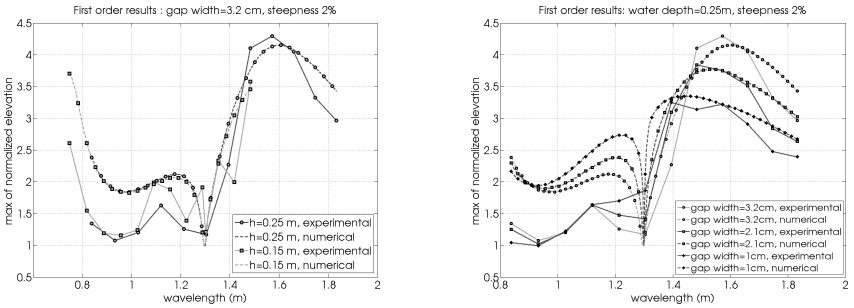

(a)Results for a gap width $d = 3.2\,\mathrm{cm}$ and water depth $h = 0.25,\ 0.15\,\mathrm{m}$.

(b)Results for a water depth $h = 0.25\,\mathrm{m}$ and gap width $h = 3,\ 2,\ 2.1,\ 1\,\mathrm{cm}$.

FIG. 5. Numerical and experimental results at first oder.

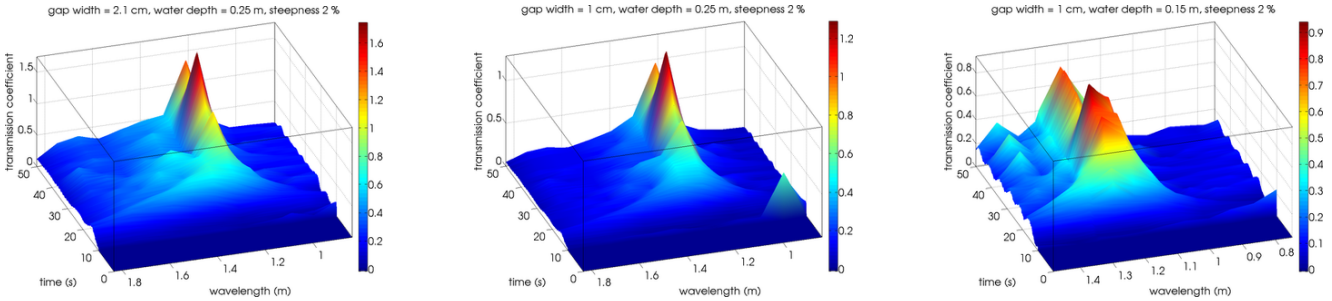

(a)Transmission coefficient for $d = 2.1\,\mathrm{cm}$ and $h_0 = 0.25\,\mathrm{m}$

(b)Transmission coefficient for $d = 1\,\mathrm{cm}$ and $h = 0.25\,\mathrm{m}$

(c)Transmission coefficient for $d = 1\,\mathrm{cm}$ and $h = 0.15\,\mathrm{m}$

FIG. 6. Transmission coefficient for different values of the narrow channel width and water depth.

IV. CONCLUSION.

We provide in this paper a study of a narrow channel in a flume for weakly nonlinear water waves at first and second order. A further work consists to use a Boussinesq type model [2] to describe wave propagation for this problem.

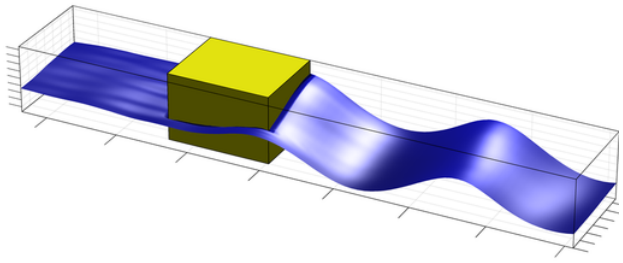

FIG. 7. Numerical simulation with a Boussinesq model.

[1] T. W. Ebbesen, H. J. Lezec, H. F. Ghaemi, T. Thio1 and P. A. Wolff, *Extraordinary optical transmission through sub-wavelength hole arrays*, Nature **391**, 667 (1998).

[2] Bingham, H.B., Madsen, P.A. & Fuhrman, D.R. *Velocity potential formulation formulations for highly accurate Boussinesq-type models.* Coast. Eng., (2009)